

Efficient electron heating in nitrogen clusters irradiated with intense femtosecond laser pulses

S. Namba,^{1,*} N. Hasegawa,² K. Nagashima,² T. Kawachi,² M. Kishimoto,² K. Sukegawa,² and K. Takiyama¹
¹Graduate School of Engineering, Hiroshima University, 1-4-1 Kagamiyama, Higashi-Hiroshima, Hiroshima 739-8527, Japan
²Advanced Photon Research Center, Japan Atomic Energy Research Institute, 8-1 Umemidai, Kizu-cho, Sourakugun, Kyoto 619-0215, Japan

(Received 10 August 2005; published 31 January 2006)

Properties of nitrogen cluster plasmas produced by an intense, ultrashort laser pulse have been investigated numerically and experimentally. The classical dynamics simulations show that on increasing the cluster size a plasma with residual electron energy above 1 keV can be created due to collisional heating, which is considerably higher than the value obtained with a conventional low-density gas target. Experimentally, nitrogen gas jets created by two types of nozzles were irradiated with a laser pulse of 55 fs, up to 1.2×10^{17} W/cm². A seeded gas jet consisting of nitrogen and helium was also employed to promote the production of large clusters. The influences of the shape of nozzle, the seeded gas, and the gas jet stagnation pressure on the properties of plasmas were examined by spectroscopic observations. *K*-shell emissions showed that for the gas jet using the conical nozzle the electrons underwent intense collisional heating within the large clusters, resulting in the production of highly charged ions. In contrast, the emissions observed with the capillary nozzle exhibited the characteristics of a cold plasma without suffering substantial electron heating, indicating the absence of large clusters. That is, the differences between the two types of nozzles in the efficiency of electron heating and subsequent residual energies after the passage of the laser pulse, which are strongly dependent upon the cluster size, drastically changed the properties of the produced plasmas. The reason that for the capillary gas jet the plasma density deduced from the recombination spectra was significantly higher than the value obtained using the conical nozzle is also given by the difference in residual electron energy.

DOI: [10.1103/PhysRevA.73.013205](https://doi.org/10.1103/PhysRevA.73.013205)

PACS number(s): 36.40.Gk, 07.05.Tp, 52.50.Jm

I. INTRODUCTION

Recently, cluster plasmas produced by intense, femtosecond laser pulses have attracted a great deal of interest for potential applications in x-ray sources [1], particle acceleration [2], and neutron sources from nuclear fusion reaction [3].

The most prominent difference between atomic cluster and gaseous targets subjected to ultrashort laser pulses arises from the heating mechanism underlying the production of high-energy electrons and highly charged ions. Since the internal density in a cluster is near the solid density, numerical calculations on the basis of the “nanoplasma” model have shown that efficient absorption of the laser pulse via collisional heating (inverse bremsstrahlung) within the clusters would result in the creation of a hot, dense cluster plasma [4]. Actually, when a deuterium cluster was irradiated with an ultrashort laser pulse, the production of ions of energies up to 1 MeV has been observed, which is high enough to induce the D-D nuclear fusion reaction [3]. On the other hand, for a low-density gas target, the collisional heating will be suppressed due to infrequent electron-ion collisions, and thus the residual electron energy after the passage of the laser pulse is described by the above-threshold ionization (ATI) energy. Therefore, it is expected that the cold ATI electrons generated will play an essential role in realizing a recombination pumping x-ray laser in an optical field ionization (OFI) plasma [5,6].

Further insight into the expansion dynamics as well as the heating mechanism of nanocluster plasmas has been obtained using the nanoplasma model [4], molecular dynamics simulations [7,8], and particle-in-cell (PIC) codes [9,10]. The nanoplasma model developed by Ditmire *et al.* [4] has shown fairly good agreement with the experimental results [11,12], in which inverse bremsstrahlung plays an important role in the production of a high-temperature plasma. A recent numerical study by Magi *et al.* [13], however, has indicated that the electron-surface collision contributes to enhancing the electron collision frequency, and thus the plasmon resonance was overestimated in the nanoplasma model. On the other hand, a classical dynamics simulation by Ishikawa *et al.* [8] has identified the explosion dynamics of small clusters, and successfully explained the asymmetric ion emission from a Xe cluster in intense laser fields, which was observed experimentally [14]. In addition, a three-dimensional (3D) microscopic PIC code developed by Jungreuthmayer *et al.* [15] has revealed that the macroscopic electric field induced in and around the cluster due to polarization caused dephasing between the laser-driven motion of the electrons and the laser field, resulting in laser-dephasing heating. However, since no numerical method that is capable of simultaneously taking into account all of the microscopic, macroscopic, and expansion phenomena has been proposed so far, the interaction of clusters with ultrashort, high-intensity pulses is still an open question.

On the other hand, various experimental researches have been carried out using time-of-flight measurements of ions and electrons and emission spectroscopy. Spectroscopic observations provide useful methods to elucidate not only the expansion dynamics of cluster plasmas but also the ioniza-

*Email address: namba@hiroshima-u.ac.jp

tion and recombination processes. Moreover, the properties of expanding plasmas, such as electron density and temperature, immediately and well after the laser pulse can be deduced from spectral analysis. Ditmire *et al.* observed the soft x-ray emissions from Ar and Kr cluster plasmas to identify the ionization processes and heating mechanism within the clusters responsible for the production of highly charged ions [4]. In addition, the long-lived x-ray emissions arising from collisional excitation in the initial hot, dense cluster plasma and the subsequent low-density, cold bulk plasma were observed using an x-ray streak camera. The temporal emission behavior observed was in fairly good agreement with the simulation of cluster plasmas on the basis of relatively simple assumptions. Moreover, Junkel *et al.* analyzed Ar *K*-shell spectra associated with the interaction of Ar clusters with a 45 fs, high-intensity laser pulse [16]. Comparison of the experimental intensity with that derived from a collisional-radiative model has indicated that there existed a small number of energetic electrons (~ 5 keV), and a plasma with the supercritical density around $2 \times 10^{22} \text{ cm}^{-3}$ was demonstrated.

We have studied the nitrogen cluster plasma produced by interaction with an ultrashort, high-intensity laser pulse. The reason why the nitrogen cluster was chosen is that compared with heavy rare-gas clusters such as Kr and Xe, the atomic structure is even simpler, and discrete line emissions from highly charged ions can be assigned easily. In addition, the high-density nitrogen plasma generated by ultrashort laser pulses has been recognized to be a promising medium from the viewpoint of OFI x-ray lasers [17].

On the other hand, the nitrogen plasma is also of interest as the lasing medium of an alternative pumping scheme for x-ray lasers [18]. Chichikov *et al.* have proposed a charge-exchange recombination scheme, in which the intrinsic character of the cluster would provide favorable conditions for population inversion [19]. In the case of a mixture of clusters and atomic gas subjected to ultrashort laser pulses, the cluster should be heated up due to collisional heating and ionized to highly charged ions, whereas atoms that do not undergo condensation should be neutral or ionized to a lower-charged stage, in which tunneling ionization dominates over the ionization processes. For nitrogen clusters and helium atoms, the charge-exchange recombination $\text{N}^{7+} + \text{He} \rightarrow \text{N}^{6+}(n=4) + \text{He}^+$ [20] is the most attractive reaction as the pumping process required for soft x-ray lasers. Since the reaction has a large cross section ($\sim 10^{-15} \text{ cm}^2$) [21], population inversions between $n=4$ and the lower levels were expected. The expected lasing wavelengths are 1.9 and 9.9 nm for N^{6+} $n=1-4$ and $n=2-4$ transitions, respectively. According to the barrier suppression ionization (BSI) model [22,23], the threshold intensity to ionize He atoms is evaluated to be $1.5 \times 10^{15} \text{ W/cm}^2$, while for large nitrogen clusters of 10 000 atoms/cluster subjected to ultrashort pulses with this intensity, the averaged residual electron energy after the passage of the laser pulse will reach 170 eV. As a result, a strongly nonequilibrium plasma that consists of highly charged nitrogen ions and He atoms is likely to be attained without difficulties on interpenetration of both species.

The purpose of this study is to investigate the properties of nitrogen cluster plasmas produced by an intense, ul-

trashort laser pulse. In Sec. II, the method of our simulation based on a classical particle-dynamics approach to study the laser-cluster interaction and the results of its numerical implementation are described. In Sec. III, the nozzles used for the creation of clusters and the seeding technique employed to enhance the clustering efficiency are presented. In Sec. IV, we show that spectroscopic observations of *K*-shell emissions provide useful information to understand that the difference in the efficiency of electron heating via inverse bremsstrahlung at the early stage using two types of nozzles, which is dependent upon the cluster size, drastically changes the properties of the plasmas produced. Also, the electron temperature and density in the recombination stage well after the laser irradiation will be presented. The conclusions will be given in Sec. V.

II. SIMULATION OF CLUSTER PLASMAS

In order to understand the dynamics of heating and ionization in clusters subjected to an ultrashort, high-intensity laser pulse, we have developed a Monte Carlo classical particle code which has been recognized to be a useful method to study the laser-cluster interaction [7,8]. The trajectories of ions and electrons exposed to the laser and the Coulomb fields acting from all the other particles can be traced by solving the relativistic equations of motion for them, in which the Lorentz factor $\gamma = [1 - (\nu/c)^2]^{-1/2}$, representing the relativistic effect, is taken into account. The relativistic treatment, however, makes no significant difference at the laser intensity with which we are concerned in this study. As for the ionization process, tunneling ionization given by the Ammosov-Delone-Krainov theory [24] was incorporated in the program, while for electron impact ionization the empirical Lotz formula [25] was also used. The actual ionization event and the position of the electron ejected from the atom and ion are calculated by the Monte Carlo technique. The electron energy just after the ionization is expressed by the ATI energy, which depends on the laser phase when the ionization takes place. At $t=0$, atoms in the cluster are arranged in space with the appropriate internuclear distance. By solving the momentum equation for the individual particle, the energy and position of the particles at time t can be determined.

On the other hand, we neglect the interaction of the relevant cluster with particles emitted from another cluster. Eloy *et al.* [26] studied a multicluster system using relativistic 2D and 3D PIC codes, in which hydrogen and argon clusters were irradiated with ultrashort, high-intensity laser pulses of 20 fs, $I = 10^{17} - 10^{20} \text{ W/cm}^2$. It was found that the presence of another cluster in the gas jet greatly influences the maximum ion energy for high-intensity laser irradiation. In the case of lower intensity, however, it seems to be insignificant.

Figure 1 shows the temporal evolutions of averaged electron and ion energies under a linear-polarized laser pulse with $\lambda = 800 \text{ nm}$, pulse width $\tau_{\text{pulse}} = 50 \text{ fs}$ with Gaussian shape, laser intensity of $I = 1.2 \times 10^{17} \text{ W/cm}^2$, and nitrogen cluster size of $N_{\text{cluster}} = 100$ atoms/cluster. Since the internal density of the cluster is sufficiently high ($7.1 \times 10^{22} \text{ cm}^{-3}$),

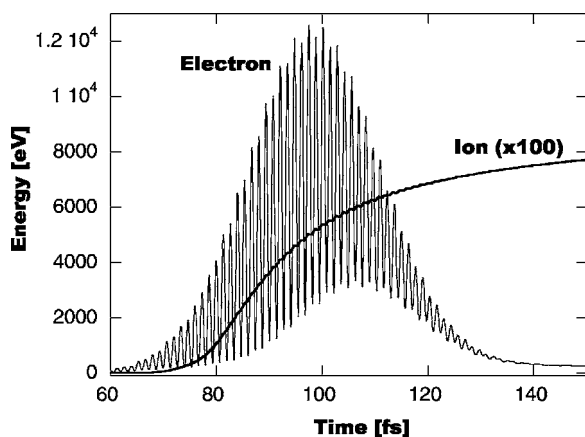


FIG. 1. Temporal evolutions of averaged electron and ion energies for nitrogen cluster ($N_{\text{cluster}}=100$ atoms/cluster) irradiated with $\lambda=800$ nm, $\tau_{\text{pulse}}=50$ fs, $I=1.2 \times 10^{17}$ W/cm² laser pulse. Ion energy is multiplied by 100.

the electrons efficiently absorb the laser energy via the Coulomb collision (inverse bremsstrahlung). Here, the averaged electron energy is given by the sum of laser-driven and thermal electron energies. The pure thermal electron energy can be obtained by tracing each bottom point of the oscillating energy curve. Although the electrons expand from the cluster at the early stage of the interaction, their motions can still be restricted due to the strong laser field, resulting in the quivering motions around the cluster core. The collisional heating, therefore, might be effective even at the peak intensity. The average electron energy at the peak laser intensity reaches ~ 12 keV and then decreases toward the averaged residual electron energy $\langle \varepsilon \rangle = 267$ eV. In order to examine the dependences of plasma temperature on the cluster size and laser intensity, the averaged residual electron and ion energies after the laser pulse were calculated. Figure 2 shows the calculated residual energies, (a) cluster size dependence for $I=1.2 \times 10^{17}$ W/cm², $\tau_{\text{pulse}}=50$ fs, (b) laser intensity dependence for $\tau_{\text{pulse}}=50$ fs, $N_{\text{cluster}}=1000$. On increasing the cluster size, the residual energies also increase, reaching above 1 keV at $I=1.2 \times 10^{17}$ W/cm² and $N_{\text{cluster}}=10\,000$. Even in moderate laser intensity such as $I=1 \times 10^{16}$ W/cm², the collisional heating contributes to increasing the kinetic energies, as shown in Fig. 2(b).

On the other hand, for a single atom or small cluster with a few atoms irradiated by ultrashort laser pulses, the ionization process is primarily dominated by the tunneling ionization due to the strong laser electric field, since the density is low enough to suppress the collisional heating. The residual energy of electrons, therefore, is expressed by the ATI energy [27], in which the electron energy distribution has a non-Maxwellian shape and a peak at residual energy of zero. As shown in Fig. 2(a), for $N_{\text{cluster}}=3$ the residual electron energy is evaluated to be $\langle \varepsilon \rangle = 44$ eV, which is almost the same value as the ATI energy of a single atom (45 eV) [28]. As a result, a significant high-intensity laser is required to produce fully stripped nitrogen ions in a gaseous target without large clusters. The increase of the atomic density in the gas jet, however, causes this situation to drastically change due to the collisional heating in an underdense plasma, even when

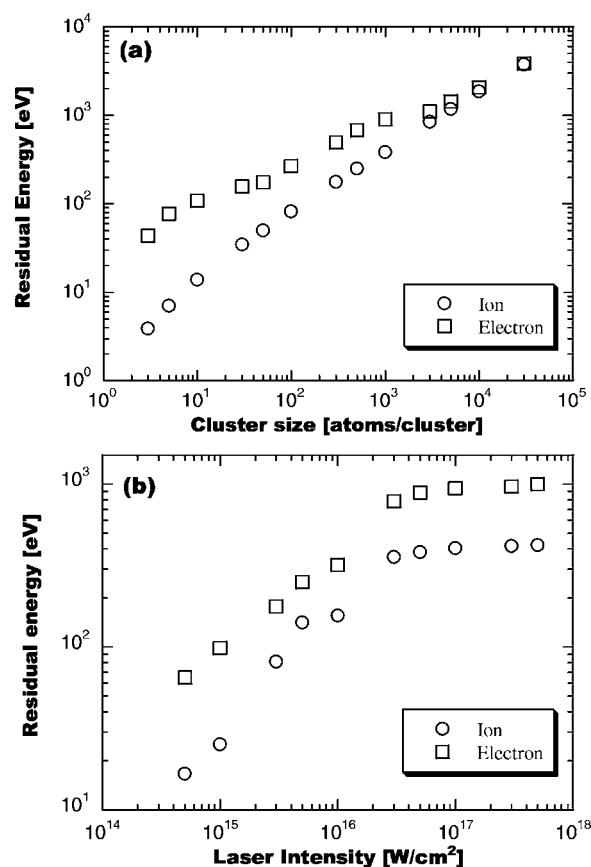


FIG. 2. Dependence of the residual electron and ion energies on (a) cluster size ($I=1.2 \times 10^{17}$ W/cm²) and (b) laser intensity ($N_{\text{cluster}}=1,000$).

large clusters are absent. Since the collision frequency of electron and ion is in proportion to $T_e^{-3/2}$ [29], the cold ATI electron produced by the optical field ionization is favorable to Coulomb collision. A numerical calculation by Ditmire has shown that inverse bremsstrahlung in a plasma ion density above around 10^{19} cm⁻³ plays an important role in rapidly increasing plasma temperature [30]. Our calculations also exhibit that the residual electron energies for nitrogen gas densities of 2×10^{19} and 2×10^{20} cm⁻³ increase to around 90 and 470 eV, respectively, at the laser intensity of 1.2×10^{17} W/cm².

III. EXPERIMENTAL SETUP

The experiment was carried out with a Ti-sapphire laser operated at $\lambda=800$ nm at JAERI Kansai. The pulse width was measured to be about 55 fs with an autocorrelator. The spot size focused with a $f/10$ lens with a 50 cm focal length was around $50 \mu\text{m}$. The maximum laser intensity on target was $I=1.2 \times 10^{17}$ W/cm². The contrast between the prepulse and the main pulse was about 10^5 .

Nitrogen cluster targets were created with pulsed supersonic nozzles. When high-density gas is injected into the vacuum, atoms bonded together by van der Waals force are produced due to cooling associated with an adiabatic expansion. Moreover, it is well known that clustering can be

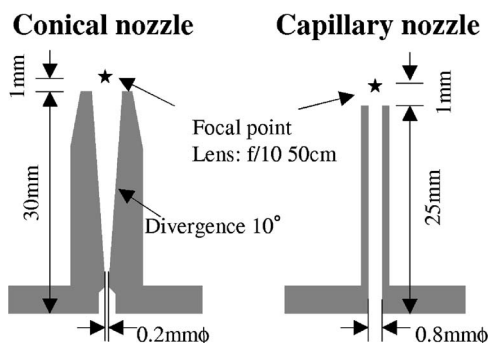


FIG. 3. Schematic diagram of gas jet nozzles: (a) conical and (b) capillary nozzle. The laser pulse was focused onto the gas jet at a distance of around 1 mm from the nozzle exits.

greatly enhanced using a conical nozzle with a throat between converging and diverging sections. In order to study the influence of the nozzle shape on clustering efficiency, a conical type nozzle with 0.2 mm ϕ throat and a capillary type nozzle with 0.8 mm ϕ were used (see Fig. 3). The laser pulses were focused onto the gas jet at a distance of around 1.0 mm from the nozzle exits. The gas density adjacent to the capillary nozzle exit under the backing pressure $P_b=15$ atm was determined to be around 2×10^{19} cm $^{-3}$ by an interference measurement with a He-Ne laser, while for the conical nozzle the average gas density on the jet axis was about 1×10^{17} cm $^{-3}$ at the same stagnation pressure, which was estimated from spatial distribution of the gas density measured with a fast ionization gauge. The average cluster sizes can be estimated by the Hagena empirical law [31]. The average sizes of $N_{\text{cluster}} \sim 12\,000$ and 1500 atoms/cluster at the nitrogen pressure of $P_b=15$ atm are expected for the conical and capillary nozzles, respectively.

On the other hand, a seeding technique was applied to promote the formation of larger clusters [32]. In a gas mixture consisting of a low concentration of heavy seed gas (nitrogen) in light carrier gas (helium), the characteristics of the supersonic beam are dominated by the more abundant lighter gas. This method, therefore, allows the seed gas to be accelerated to the beam velocity of the carrier gas and also allows the internal degrees of freedom of the heavier gas to be cooled considerably. Moreover, it is shown that the heavier species tend to concentrate on the gas jet axis. As a result, the enhancement of clustering efficiency, leading to the creation of large clusters, can be expected. Actually, the advantage of the seeding method was confirmed by Rayleigh scattering measurements in the admixture gas jet [4]. In order to examine the effect of the seeding method, i.e., the presence of large clusters in the gas jet, on the properties of the plasmas produced, the partial pressures of nitrogen to helium gas of 30, 50, 70, and 100 % were employed in the present study.

Soft x-ray emission from the laser-produced plasmas was measured using a grazing-incidence spectrometer with a flat field grating (1200 lines/mm) in a direction perpendicular to the laser propagation. A gold-coated spherical mirror with curvature of 3520 mm was used to collect the x-ray emission. The detectors were a back-illuminated charged coupled device (CCD) camera for time-integrated measurements and

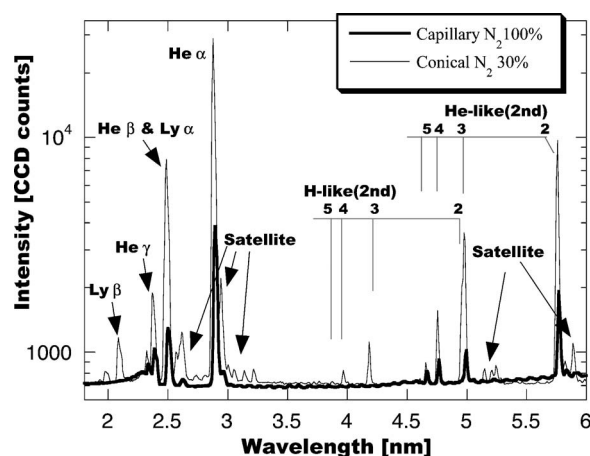


FIG. 4. H-like and He-like emissions from the nitrogen plasma produced by irradiation of 55 fs, $I=1.2 \times 10^{17}$ W/cm 2 laser pulse onto the gas jet ($P_b=23$ atm). For the conical nozzle, the seeding fraction was N $_2$ 30% and He 70%, while for the capillary, N $_2$ 100%, at which intense emissions were observed.

an x-ray streak camera for the measurement of the time-resolved spectrum. The quantum efficiency of the CCD camera and the diffraction efficiency of the grating were taken into account in deriving the relative spectral intensities of H-like, He-like, and Li-like nitrogen ions.

IV. EXPERIMENTAL RESULTS AND DISCUSSION

A. Analysis of H- and He-like ion spectra

Figure 4 shows the emission spectrum from the nitrogen plasma produced by the conical nozzle (mixture of N $_2$ 30% and He 70%) under the backing pressure of $P_b=23$ atm and the laser intensity $I=1.2 \times 10^{17}$ W/cm 2 . In this wavelength region, the Lyman series of H-like and He-like nitrogen ions and He-like and Li-like satellite lines were observed. Since the average gas density at the focus point of the laser pulse was low enough ($\sim 10^{17}$ cm $^{-3}$) for the conical nozzle, the atoms and ions should be predominantly ionized via the tunneling ionization process in a strong laser field. According to the BSI model [22,23], however, the threshold intensity required to generate H-like ions corresponds to 1×10^{19} W/cm 2 , over two orders of magnitude in excess of the present laser intensity. Also, it is important to note that only highly charged ions up to the ground state of He-like ions can be produced by field ionization. Nevertheless, the fact that H-like ion spectra as well as He-like ones were observed with the conical nozzle suggests that the large cluster should be formed in the gas jet, resulting in the creation of high-temperature cluster plasmas due to the efficient deposition of laser energy within the clusters.

Further evidence of the appearance of large clusters in the gas jet of the conical nozzle is provided by the behavior of He-like emissions under the seeded gas injection consisting of the admixture gas of nitrogen and helium. Figure 5 shows the dependences of the emission intensities of He- α and β and γ of nitrogen on the partial pressure of nitrogen under $P_b=15$ atm and $I=1.2 \times 10^{17}$ W/cm 2 . It is of great signifi-

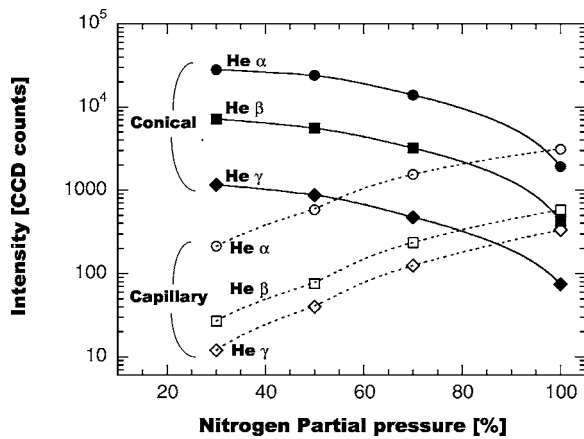


FIG. 5. Seeding effect on He-like intensities under the experimental conditions of 1.2×10^{17} W/cm² and $P_b=15$ atm. For the conical nozzle, the bright emissions were obtained at N₂ 30% due to the appearance of large cluster, while for the capillary nozzle the fraction of N₂ 100% was preferable for the intense emission.

cance to note that the He-like spectra are one of the measures of whether the high-temperature plasma is generated, since the excitation energy of $E=430$ eV is required for the production of He-like $2p$ levels. For the conical nozzle, the bright emissions have been obtained at the fraction of N₂ 30%. Considering that the seeding method enhances clustering efficiency, the result obtained indicates that the larger cluster necessary to produce higher-temperature plasma as shown in Fig. 2(a) should be formed in the conical gas jet with decreasing partial pressure of nitrogen.

On the other hand, for the capillary nozzle (N₂ 100%, $P_b=23$ atm), the H-like Ly series and satellite lines cannot be observed as shown in Fig. 4, indicating that the electron temperature was not high enough to create the excited states of H-like ions. Moreover, contrary to the results obtained using the conical nozzle, the intense emissions of He-like ion were observed at the fraction of N₂ 100% as shown in Fig. 5. This probably implies that there did not exist a large cluster in the capillary gas jet, even with the aid of the seeding method at $P_b=15$ atm. The reason that the nitrogen did not undergo clustering efficiently for the capillary nozzle may be that the adiabatic cooling early in the expansion was not sufficient to grow the large cluster. The laser pulse, therefore, did not interact with large clusters but mainly with the high-density gas and small clusters. Although the tunneling process would produce cold bulk electrons whose energies are not high enough to generate the excited levels of He-like ions, the result that the emissions from He-like ions can also be observed for the capillary nozzle suggests that the underdense plasma enough to heat the electrons due to inverse bremsstrahlung could be generated. As will be described later, the plasma density for the capillary nozzle was found to be about 10^{19} cm⁻³, around which the collisional process begins to contribute to the heating of electrons [30,33], and hence this interpretation is reasonable in describing the heating mechanism responsible for the production of He-like excited levels in the capillary gas jet. However, considering that the intensities of He-like ions observed using the capillary nozzle were considerably low compared with those ob-

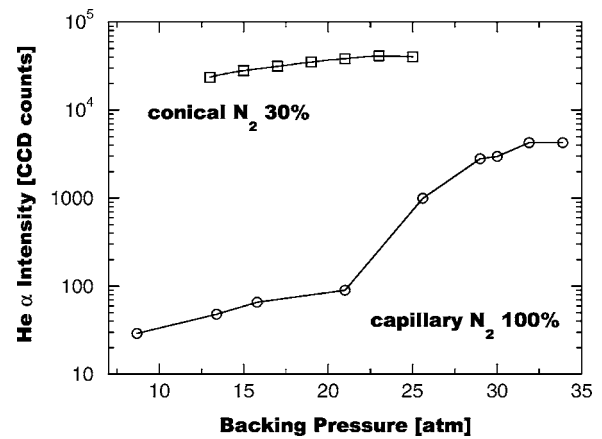


FIG. 6. Dependence of He- α intensity on the backing pressure of gas jet at the laser intensity of 9×10^{16} W/cm². The fractions of N₂ in the admixture gases were 30% for the conical and 100% for the capillary nozzles.

tained by the conical jet, significant electron heating sufficient to allow the production of a large amount of H-like ions as well as He-like excited levels is not likely to take place for the capillary nozzle as shown in the previous section.

The next discussion concerns the influence of the gas jet backing pressure on the properties of the produced plasma. According to the Hagena empirical law, the average cluster size against the stagnation pressure increases in proportion to $P_b^{2.35}$ [31]. Figure 6 shows the dependence of the He- α intensity of nitrogen on the backing pressure under the fraction of N₂ 30% for the conical nozzle and N₂ 100% for the capillary at the laser intensity of 9×10^{16} W/cm². For the conical nozzle, the He- α intensity is almost saturated and tends to be rolled over at $P_b=25$ atm, which may be explained by the existence of an optimum cluster size for heating the electrons within clusters as reported in Ref. [4]. Meanwhile, for the capillary nozzle the intensity drastically increased by an order of magnitude at $P_b=25$ atm, around which the large clusters may begin to be formed in the capillary gas jet.

In order to understand the temporal behavior of the plasma, measurements using the x-ray streak camera were also performed. Figure 7 shows the temporal evolution of the He- α intensity observed for the conical gas jet under the conditions of $P_b=15$ atm and N₂ 30%. The origin of the time on the abscissa axis was determined by a fast photodiode detector, and the timing jitter of laser pulses was around 400 ps. The other emission lines of He-like and H-like ions observed exhibited similar behaviors. For the capillary nozzle, no signal was observed because of the weak emission. In spite of the laser pulse width of 55 fs, the spectral intensity began to rise around 1 ns after the laser irradiation, and then disappeared around 1.8 ns. The cluster expansion time in the present study is evaluated to be shorter than 1 ps [4], and hence the hot, overdense cluster plasma evolves into a cold, underdense plasma immediately after the laser pulse. Consequently, it is reasonable to suppose that the x-ray emission observed reflects the property of the recombining plasma formed well after the clusters expand, rather than that of the plasma produced during and immediately after the laser irradiation. This feature also implies that the time-

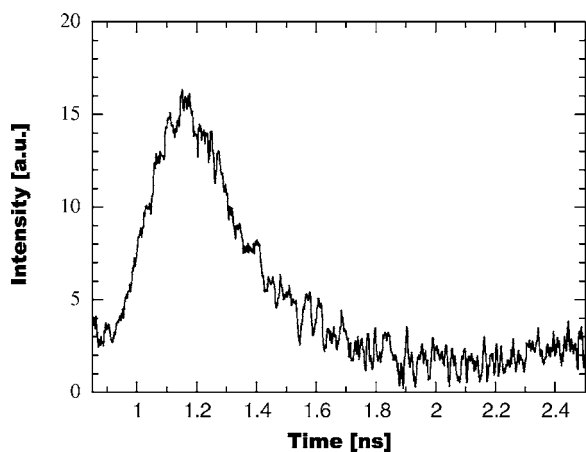


FIG. 7. Temporal evolution of He- α intensity observed using the streak camera. The measurement was performed with the conical nozzle at 1.2×10^{17} W/cm 2 and $P_b=15$ atm (N_2 30%).

integrated spectrum observed using the CCD camera gives information on the recombining plasma whose temperature should be considerably lower than that in the initial stage.

Plasma parameters such as the electron density and temperature were deduced from a comparison of the experimental spectral intensities with the values calculated by a collisional-radiative model. A program to calculate the population densities of the excited levels of H-like ions, COLRAD, by Ljepojevic *et al.* [34], was used. Here, it should be noted that the high plasma density makes the resonance lines opaque, thus having a great influence on the population densities in the optically thick plasma. The equation of radiation transfer, therefore, has to be solved simultaneously with the rate equations to accurately estimate the population densities. In the present study, we adopt the approximation that the effective transition probability $\Lambda_{ik}A(k,i)$ for the spontaneous transition $A(k,i)$ represents the effect of the radiation trapping [35], where Λ_{ik} is the optical escape factor for the transition from k to i levels. For simplicity, we assume that the spectral profile has a Lorentzian shape due to the Stark effect in the high-density plasma, and the plasma has a cylindrical geometry with homogeneous distribution [36,37]. After the individual cluster is decomposed, the expanding electrons and ions may be thermalized in collision with the particles expanding from other surrounding clusters. Therefore, the assumption on the cylindrical plasma with spot size and Rayleigh length is probably justified [4]. The Stark width under the quasistatic approximation that is given by Griem [38] was also incorporated to estimate the optical depth at the line center [37]. The calculated intensity corresponding to the transition from k to i levels is given by $n(k)A(k,i)\Lambda_{ik}$, where $n(k)$ is the population density of level k . In calculation, the only recombining component which is in proportion to the density of the fully stripped ion was taken into account. This assumption is correct, because the plasma emission was observed in the recombination stage well after laser pulse. Meanwhile, since the blending of H-like Ly- α with He- β spectra prevents us from determining their intensities accurately, the corresponding third-order spectra were analyzed to derive the Ly- α intensity. Figure 8 shows the normalized

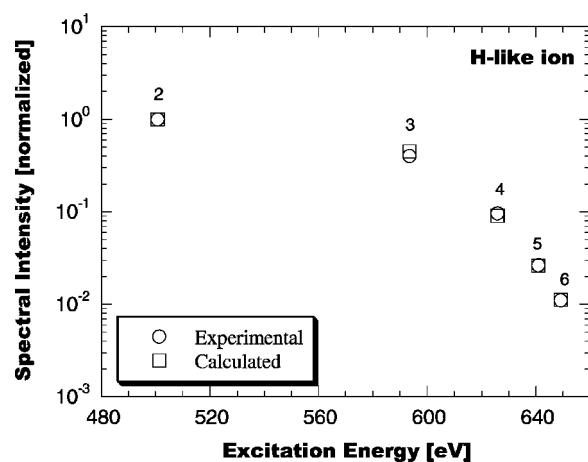


FIG. 8. Comparison of the experimental H-like intensities with the values calculated using the collisional-radiative model. The plasma parameters of $n_e=2 \times 10^{19}$ cm $^{-3}$, $T_e=20$ eV, the H-like ground density 5×10^{18} cm $^{-3}$, and plasma radius $25 \mu\text{m}$ were used for the calculation.

intensities of H-like Ly series obtained using the conical nozzle ($P_b=15$ atm, N_2 30%) and the calculated values for the conditions of $n_e=2 \times 10^{19}$ cm $^{-3}$, $T_e=20$ eV, the H-like ground density 5×10^{18} cm $^{-3}$, and plasma radius $25 \mu\text{m}$. Good agreement between the intensity distributions derived from the calculation and the experimental values has been achieved. Here, the optical escape factors of Ly- α and Ly- β transitions were calculated to be $\Lambda_{12}=0.21$ and $\Lambda_{13}=0.76$, respectively, showing that strong radiation trapping did not take place due to the small radius plasma and broadened spectral profile. If we assume a Gaussian profile with the ion temperature of 20 eV ($=T_e$) as the spectral profile, the optical thickness drastically increases to $\Lambda_{12}=3.4 \times 10^{-2}$ and $\Lambda_{13}=0.33$ due to the narrower Doppler profile.

As for the He-like ion, the K -shell spectroscopy code FLY [39] was employed to determine the plasma parameters. In order to calculate the population densities in the recombining plasma under quasi-steady-state approximation, the source code was modified in the present study. Figure 9 shows the observed and calculated intensities of He-like resonance lines for (a) the conical (N_2 30%) and (b) capillary nozzle (N_2 100%) at $P_b=15$ atm. The parameters in calculations were the following: $n_e=5 \times 10^{18}$ cm $^{-3}$, $T_e=10$ eV, and He-like ground density 1×10^{18} cm $^{-3}$ for the conical nozzle, and $n_e=5 \times 10^{19}$ cm $^{-3}$, $T_e=30$ eV, and He-like ground density 1×10^{19} cm $^{-3}$ for the capillary. Here, the electron temperature derived from the radiative recombination continuum spectra was used for the capillary nozzle. Attenuation of x rays through the nitrogen gas was also taken into account by assuming the absorption medium of the pressure $P=10$ Torr and the length $L=2$ mm for the conical, and $P=300$ Torr, $L=1$ mm for the capillary nozzle. In both cases, the calculated results are successful in reproducing the experimental values. The density obtained using the capillary is also in good agreement with density determined using an interferometer in a nitrogen gas jet subjected to an ultrashort pulse laser [17].

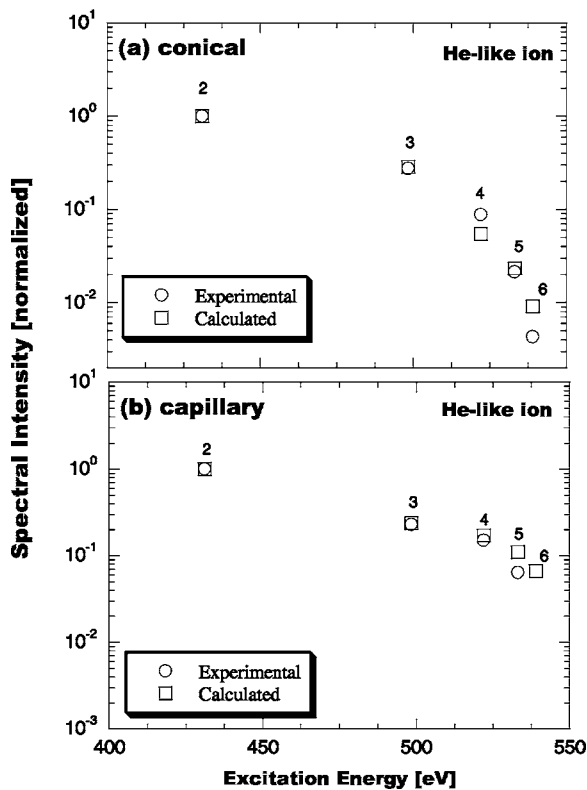


FIG. 9. Comparison of the experimental He-like intensities with the calculated values under the condition of (a) $n_e=5 \times 10^{18} \text{ cm}^{-3}$, $T_e=10 \text{ eV}$, and He-like ground density $1 \times 10^{18} \text{ cm}^{-3}$ for the conical nozzle, and (b) $n_e=5 \times 10^{19} \text{ cm}^{-3}$, $T_e=30 \text{ eV}$, and He-like ground density $1 \times 10^{19} \text{ cm}^{-3}$ for the capillary.

Here, the question we have to ask is why the electron density of the plasma produced by the capillary nozzle is by an order of magnitude higher than the value obtained using the conical nozzle. The reason for this is probably given by the differences in the efficiency of electron heating and subsequent residual energies after the passage of a laser pulse between two nozzles. For the conical nozzle, the electron temperature, which is expected to attain above 1 keV in the early stage due to the appearance of large clusters, is too high for electrons to recombine with ions. For example, assuming the parameters of $n_e=1 \times 10^{21} \text{ cm}^{-3}$ and $T_e=1 \text{ keV}$ after the laser pulse, the collisional-radiative model gives that the ionization and recombination rate coefficients of H-like ions are $S=1.8 \times 10^{-10}$ and $\alpha=1.7 \times 10^{-13} \text{ cm}^3/\text{s}$, respectively. As a result, the recombination process takes place in a sufficiently later stage after the laser irradiation, at which the clusters are completely disassembled and the low-temperature and underdense plasma responsible for the intense emissions can be formed. This interpretation is consistent with the behavior of the temporal evolution of the spectrum. Meanwhile, for the capillary nozzle the residual electron energy predicted by numerical calculation corresponds to around 90 eV, if the cluster is not present in the gas jet. For $n_e=1 \times 10^{20} \text{ cm}^{-3}$, $T_e=90 \text{ eV}$, the recombination coefficient increases to $\alpha=3.8 \times 10^{-12} \text{ cm}^3/\text{s}$, while the ionization coefficient $S=7.0 \times 10^{-13} \text{ cm}^3/\text{s}$. Therefore, the recombination process dominates over the ionization and is likely to begin to take

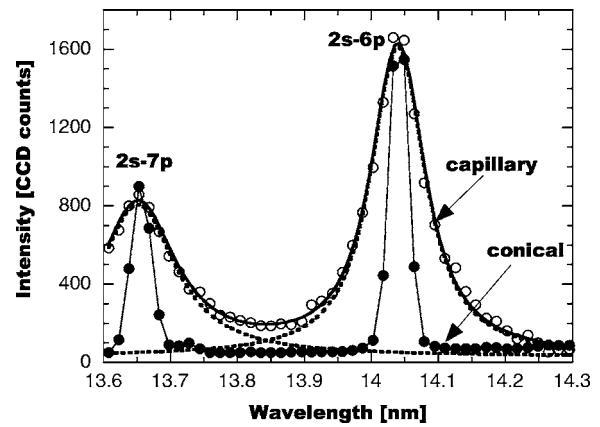


FIG. 10. Stark broadenings of $2s-6p$ and $2s-7p$ transitions. The observed Li-like ion spectra, the deconvoluted spectra, and their sum are represented with the open circles, the dotted curves, and the solid curves, respectively. The experimental condition for the capillary gas jet was $P_b=15 \text{ atm}$ (N_2 100%) and $I=1.2 \times 10^{17} \text{ W/cm}^2$. For reference, the spectrum obtained by the conical nozzle (N_2 30% at 15 atm) is also shown with the closed circles.

place immediately after the passage of the laser pulse. In addition, the cold ATI electrons that may be still present in high-density plasma without undergoing collisional heating may enhance the recombination rate [30]. Consequently, the emissions observed with the capillary gas jet reflect the plasma parameters in the early stage, thus indicating the characteristics of a low-temperature and high-density plasma.

B. Analysis of Li-like ion spectra

Li-like ion spectra were also observed to examine the properties of the plasmas in the recombining stage. The most prominent difference can be seen as line broadening, that is, for the capillary nozzle, the spectral lines associated with the transition from highly lying levels were significantly broadened, while the narrower line profiles were observed using the conical nozzle. This implies that the high-density plasma can be produced with the capillary nozzle, which is consistent with the results obtained by the spectral analysis of He-like ions.

The electron density for the capillary nozzle was determined from Stark broadenings of $2s-6p$ and $2s-7p$ transitions. We assume that the spectral profile is given by the Voigt function consisting of a Lorentzian shape due to Stark broadening and a Gaussian with instrumental width of 0.03 nm. The observed Li-like ion spectrum, the deconvoluted spectra for the above two transitions, and the superposition of them are represented in Fig. 10 with open circles, dotted curves, and solid curves, respectively. The experimental condition for the capillary was $I=1.2 \times 10^{17} \text{ W/cm}^2$ and $P_b=15 \text{ atm}$ (N_2 100%). Here, the optical thickness was neglected due to the transitions from highly lying levels. For reference, the spectrum obtained with the conical nozzle is also shown in the figure with the closed circles (N_2 30% at 15 atm). In the experiment, the full widths at half maximum (FWHMs) of the Lorentzian profiles were 0.087 nm for

$2s-6p$ transition and 0.129 nm for $2s-7p$, respectively. In order to estimate the electron density, the comparison with FWHMs calculated using the FLY code [40] was carried out. For the parameters of $T_e=8$ eV, $n_e\sim 3\times 10^{19}$ cm $^{-3}$, the corresponding widths were found to be 0.083 nm for the $2s-6p$ transition and 0.127 nm for the $2s-7p$, respectively.

On the other hand, an alternative method to determine the electron density was also employed. According to the Inglis-Teller relationship, the electron density is expressed by $\log_{10} n_e = 23.491 - 1.5 \log_{10} |Z_p| + 4.5 \log_{10} Z - 7.7 \log_{10} n_m$, where Z_p is the charge and Z is the atomic number [41]. The value n_m is the resolvable maximum quantum number. For the capillary nozzle under $P_b=15$ atm of N_2 100%, n_m was 8. Since the emissions reflect the characteristics of the recombining plasma in which the dominant charge state is considered to be the He-like ion, Z_p is assumed to be 5. By substituting the parameters, we obtain $n_e\sim 3\times 10^{19}$ cm $^{-3}$, which fairly coincides with the density obtained from Stark broadening. Likewise, for the conical nozzle, the electron density was $n_e=8\times 10^{17}$ cm $^{-3}$ under the experimental condition of $P_b=15$ atm and N_2 30%, which is by one order of magnitude lower compared with the value obtained with the capillary nozzle.

The comparisons of the experimental intensities with the values calculated by the collisional-radiative model were also performed for the Li-like ion. The program developed by Kawachi *et al.* [42,43] was modified to incorporate the optical thickness, in which the optical escape factor corresponding to the resonance series was calculated by a similar treatment to that of the H-like ion. The experimental and calculated intensities of $2p-nd$ series of Li-like ions are shown in Fig. 11 for (a) the capillary nozzle (N_2 100%), and (b) the conical nozzle (N_2 30%) at $P_b=15$ atm and $I=1.2\times 10^{17}$ W/cm 2 . By assuming $T_e=6$ eV, $n_e=3\times 10^{19}$ cm $^{-3}$, and the Li-like ground density 8×10^{18} cm $^{-3}$ for the capillary nozzle and $T_e=3$ eV, $n_e=1\times 10^{18}$ cm $^{-3}$ and the ground density of the Li-like ion 3×10^{17} cm $^{-3}$ for the conical, good agreement between the experimental and calculated results was obtained. The difference in the plasma densities between two gas jets is also ascribed to the heating mechanism during laser irradiation. The striking point of the results for the capillary nozzle is that the electron densities obtained by the analyses of He-like and Li-like spectra are almost the same. The reason may be found in the spatial distribution of laser intensity in the gas jet. The central region of the laser spot has a slightly high electron energy due to the collisional heating (~ 90 eV at 1.2×10^{17} W/cm 2), while for the outer region, a low energy because of the low intensity. For example, the residual electron energy is evaluated to be around 49 eV at an intensity of 1.5×10^{16} W/cm 2 which corresponds to the BSI threshold intensity to produce a He-like ground state. The cold ATI electrons responsible for the strong recombination, therefore, may be still present in the outer region of the laser spot where the dominant ion species is a He-like ion ground state. As a result, Li-like emissions probably reflect the property of the recombining plasma in the outer region, while He-like ones do it in the central region.

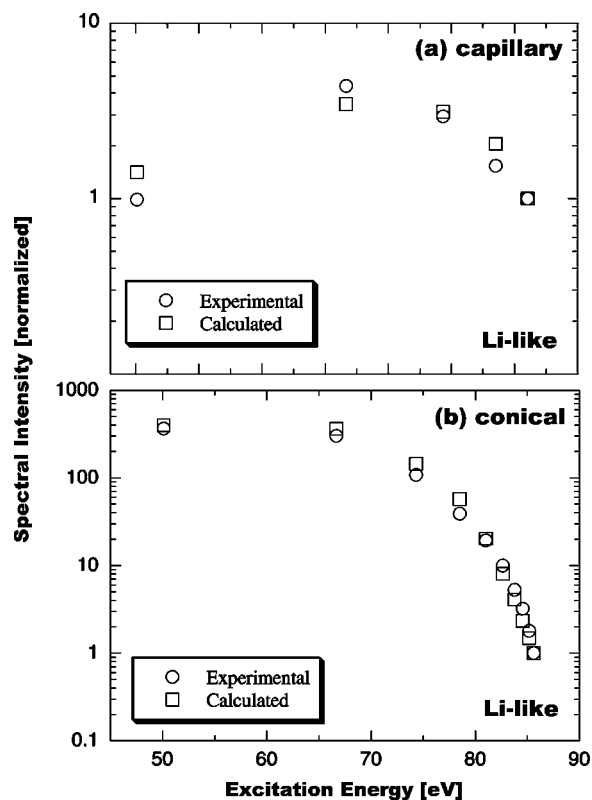


FIG. 11. Experimental and calculated intensities of Li-like ion spectra. (a) $T_e=6$ eV, $n_e=3\times 10^{19}$ cm $^{-3}$, and Li-like ground density 8×10^{18} cm $^{-3}$ for the capillary and (b) $T_e=3$ eV, $n_e=1\times 10^{18}$ cm $^{-3}$, the ground density of Li-like ion 3×10^{17} cm $^{-3}$ for the conical gas jet.

V. CONCLUSION

The properties of the nitrogen cluster plasmas produced by an ultrashort, high-intensity laser pulse have been investigated numerically and experimentally.

Classical dynamics simulations showed that the collisional heating played an important role in creating high-energy electrons after the passage of the laser pulse, since the internal density of the cluster was high enough for Coulomb collision to take place frequently. On increasing the cluster size, the residual energies of electrons and ions drastically increased, resulting in the production of high-temperature cluster plasmas. Meanwhile, for single atoms and small clusters with a few atoms, the ionization was primarily dominated by the tunneling process due to the strong laser field, yielding the cold bulk electrons whose energies could be expressed by the ATI energy.

Experimentally, the nitrogen gas jets generated by the capillary and conical types of nozzles were irradiated by 55 fs, high-intensity laser pulses up to the intensity of 1.2×10^{17} W/cm 2 . For the conical nozzle, the fact that emissions from H-like as well as He-like ions were observed suggests that the large clusters created within the gas jet interact with the laser pulse, leading to the production of a high-temperature cluster plasma due to the collisional heating. Further evidence that the large cluster existed within the gas jet was provided by the behavior of He-like emissions

under seeded gas injection. For the conical jet, intense emissions from H- and He-like ions were obtained at the fraction of N₂ 30%. This implied that the seeding served to enhance the condensation of atoms in the gas jet, followed by the creation of high-energy electrons by interaction of the large clusters with the laser pulse. For the capillary nozzle, however, we did not observe the spectrum of H-like ions, and the dependence of He-like ion emissions on the partial pressure exhibited the converse relation. The results showed that for the capillary the laser pulse did not interact with large clusters but with the high-density gas and small clusters, resulting in the production of cold ATI electrons that may not undergo substantial heating.

In order to determine the electron density and temperature in the recombining stage, a comparison of the intensity distributions of H- and He-like resonance series with values calculated by collisional-radiative models were carried out. From the distribution of H-like spectral intensities, the

plasma parameters of $n_e=2 \times 10^{19} \text{ cm}^{-3}$, $T_e=20 \text{ eV}$ were obtained for the conical nozzle ($P_b=15 \text{ atm}$, N₂ 30%), while from He-like ion spectra $n_e=5 \times 10^{18} \text{ cm}^{-3}$, $T_e=10 \text{ eV}$ for the conical (N₂ 30%) and $n_e=5 \times 10^{19} \text{ cm}^{-3}$, $T_e=30 \text{ eV}$ for the capillary gas jet (N₂ 100%) at $P_b=15 \text{ atm}$ were derived. The large difference in the electron densities between the two gas jets can be explained by the efficiency of electron heating and subsequent residual energies.

Spectra of Li-like ion were also analyzed to understand the properties of recombining plasmas. The most prominent difference between the two nozzles can be seen in broadening spectra. The Stark widths of $2s-6p$ and $2s-7p$ transitions using the capillary nozzle gave $n_e \sim 3 \times 10^{19} \text{ cm}^{-3}$ for $T_e=8 \text{ eV}$, which was consistent with the density derived from the Inglis-Teller relationship. The collisional-radiative model of Li-like ions also showed that the plasma parameters were $T_e=6 \text{ eV}$, $n_e=3 \times 10^{19} \text{ cm}^{-3}$ for the capillary and $T_e=3 \text{ eV}$, $n_e=1 \times 10^{18} \text{ cm}^{-3}$ for the conical nozzle.

-
- [1] A. McPherson, B. D. Thompson, A. B. Borisov, K. Boyer, and C. K. Rhodes, *Nature (London)* **370**, 631 (1994).
- [2] Y. L. Shao, T. Ditmire, J. W. G. Tisch, E. Springate, J. P. Marangos, and M. H. R. Hutchinson, *Phys. Rev. Lett.* **77**, 3343 (1996).
- [3] T. Ditmire, J. Zweiback, V. P. Yanovsky, T. E. Cowan, G. Hays, and K. B. Wharton, *Nature (London)* **398**, 489 (1999).
- [4] T. Ditmire, T. Donnelly, A. M. Rubenchik, R. W. Falcone, and M. D. Perry, *Phys. Rev. A* **53**, 3379 (1996).
- [5] N. H. Burnett and G. D. Enright, *IEEE J. Quantum Electron.* **26**, 1797 (1990).
- [6] S. Hulin, T. Auguste, P. D'Oliveira, P. Monot, S. Jacquemot, L. Bonnet, and E. Lefebvre, *Phys. Rev. E* **61**, 5693 (2000).
- [7] C. Rose-Petruck, K. J. Schafer, K. R. Wilson, and C. P. J. Barty, *Phys. Rev. A* **55**, 1182 (1997).
- [8] K. Ishikawa and T. Blenski, *Phys. Rev. A* **62**, 063204 (2000).
- [9] M. Eloy, R. Azambuja, J. T. Mendonça, and R. Bingham, *Phys. Plasmas* **8**, 1084 (2001).
- [10] A. Pukhov, *J. Plasma Phys.* **61**, 425 (1999).
- [11] T. Ditmire, R. A. Smith, J. W. G. Tisch, and M. H. R. Hutchinson, *Phys. Rev. Lett.* **78**, 3121 (1997).
- [12] T. Ditmire, E. Springate, J. W. G. Tisch, Y. L. Shao, M. B. Mason, N. Hay, J. P. Marangos, and M. H. R. Hutchinson, *Phys. Rev. A* **57**, 369 (1998).
- [13] F. Megi, M. Belkacem, M. A. Bouchene, E. Suraud, and G. Zwicknagel, *J. Phys. B* **36**, 273 (2003).
- [14] E. Springate, N. Hay, J. W. G. Tisch, M. B. Mason, T. Ditmire, M. H. R. Hutchinson, and J. P. Marangos, *Phys. Rev. A* **61**, 063201 (2000).
- [15] C. Jungreuthmayer, M. Geissler, J. Zanghellini, and T. Brabec, *Phys. Rev. Lett.* **92**, 133401 (2004).
- [16] G. C. Junkel-Vives, J. Abdallah, Jr., F. Blasco, F. Dorchies, T. Caillaud, C. Bonte, C. Stenz, F. Salin, A. Ya. Faenov, A. I. Magunov, T. A. Pikuz, and I. Yu. Skobelev, *Phys. Rev. A* **66**, 033204 (2002).
- [17] S. Dobosz, P. D'Oliveira, S. Hulin, P. Monot, F. Reau, and T. Auguste, *Phys. Rev. E* **65**, 047403 (2002).
- [18] E. Fill, S. Borgström, J. Larsson, T. Starczewski, C.-G. Wahlström, and S. Svanberg, *Phys. Rev. E* **51**, 6016 (1995).
- [19] B. N. Chichkov, A. Egbert, S. Meyer, B. Wellegehausen, L. Aschke, H.-J. Kunze, and Y. Kato, *Jpn. J. Appl. Phys., Part 1* **38**, 1975 (1999).
- [20] S. Namba, T. Kawachi, N. Hasegawa, K. Nagashima, K. Sukegawa, M. Kado, M. Tanaka, H. Daido, and Y. Kato, *Int. J. Appl. Electromagn. Mech.* **14**, 277 (2001).
- [21] M. Kimura, T. Iwai, Y. Kaneko, N. Kobayashi, A. Matsumoto, S. Ohtani, K. Okuno, S. Takagi, and H. Tawara, *J. Phys. Soc. Jpn.* **53**, 2224 (1984).
- [22] S. Augst, D. Strickland, D. D. Meyerhofer, S. L. Chin, and J. H. Eberly, *Phys. Rev. Lett.* **63**, 2212 (1989).
- [23] S. Augst, D. D. Meyerhofer, D. Strickland, and S. L. Chin, *J. Opt. Soc. Am. B* **8**, 858 (1991).
- [24] M. V. Ammosov, N. B. Delone, and V. P. Krainov, *Zh. Eksp. Teor. Fiz.* **91**, 2008 (1986) [*Sov. Phys. JETP* **64**, 1191 (1986)].
- [25] W. Lotz, *Z. Phys.* **216**, 241 (1968).
- [26] M. Eloy, R. Azambuja, and J. T. Mendonça, CLF Annual Report, 1999/2000 (unpublished), p. 67.
- [27] R. R. Freeman and P. H. Bucksbaum, *J. Phys. B* **24**, 325 (1991).
- [28] N. E. Andreev, *JETP Lett.* **68**, 592 (1998).
- [29] L. Spitzer, Jr., *Physics of Fully Ionized Gases* (Interscience, New York, 1962).
- [30] T. Ditmire, *Phys. Rev. E* **54**, 6735 (1996).
- [31] O. F. Hagen and W. Obert, *J. Chem. Phys.* **56**, 1793 (1972).
- [32] M. D. Morse, in *Atomic, Molecular, and Optical Physics: Atoms and Molecules*, edited by F. B. Dunning and R. G. Hulet (Academic Press, New York, 1996).
- [33] A. Sagisaka, H. Honda, K. Kondo, H. Suzuki, K. Nagashima, T. Kawachi, A. Nagashima, Y. Kato, and H. Takuma, *Appl. Phys. B: Lasers Opt.* **70**, 549 (2000).
- [34] N. N. Ljepojevic, R. J. Hucheon, and J. Payne, *Comput. Phys. Commun.* **44**, 157 (1987).
- [35] M. Otsuka, R. Ikee, and K. Ishii, *J. Quant. Spectrosc. Radiat. Transf.* **21**, 41 (1979).

- [36] S. Namba, M. Goto, H. Tsuboi, T. Oda, and K. Sato, *J. Appl. Phys.* **88**, 3182 (2000).
- [37] S. Namba, R. Nozu, K. Takiyama, and T. Oda (unpublished).
- [38] H. R. Griem, *Plasma Spectroscopy* (McGraw Hill, New York, 1964).
- [39] R. W. Lee, B. L. Whiten, and R. E. Stout, *J. Quant. Spectrosc. Radiat. Transf.* **32**, 91 (1984).
- [40] R. W. Lee, *J. Quant. Spectrosc. Radiat. Transf.* **40**, 561 (1988).
- [41] D. R. Inglis and E. Teller, *Astrophys. J.* **90**, 439 (1939).
- [42] T. Kawachi and T. Fujimoto, *Phys. Rev. E* **55**, 1836 (1997).
- [43] T. Kawachi, *Phys. Rev. E* **67**, 016409 (2003).